

Article

Open Access



# Modulating carrier-catalyst heterointerfaces to boost catalytic polysulfide conversion in lithium-sulfur batteries

Han Jin<sup>1,\*</sup>, Haojie Li<sup>1,2,#,\*</sup> , Teng Deng<sup>3,4,#</sup>, Ce Yang<sup>1</sup>, Kuming Pan<sup>2</sup>, Zhengqian Jin<sup>3</sup>, Yitong Zhang<sup>3</sup>, Saifei Pan<sup>1</sup>, Yongpeng Ren<sup>2</sup>, Yaru Li<sup>2</sup>, Xuemin Chen<sup>2</sup>, Huiyuan Yang<sup>1</sup>, Shengyu Yin<sup>5</sup>, Xuetao Wang<sup>1,\*</sup> , Kai Xi<sup>3,\*</sup>

<sup>1</sup>College of Vehicle and Traffic Engineering, Henan University of Science and Technology, Luoyang 471003, Henan, China.

<sup>2</sup>Henan Key Laboratory of High-temperature Structural and Functional Materials, Henan University of Science and Technology, Luoyang 471003, Henan, China.

<sup>3</sup>School of Chemistry, Engineering Research Center of Energy Storage Materials and Devices, Ministry of Education, National Innovation Platform (Center) for Industry-Education Integration of Energy Storage Technology, State Key Laboratory for Electrical Insulation and Power Equipment, Engineering Research Center of Energy Storage Material and Chemistry, Universities of Shaanxi Province, Xi'an Jiaotong University, Xi'an 710049, Shaanxi, China.

<sup>4</sup>School of Mechanical & Electrical Engineering, Xi'an Key Laboratory of Clean Energy, Shaanxi Key Laboratory of Nanomaterials and Nanotechnology, Xi'an University of Architecture and Technology, Xi'an 710055, Shaanxi, China.

<sup>5</sup>LB Group Co., Ltd., Jiaozuo 454191, Henan, China.

#Authors contributed equally.

**\*Correspondence to:** Prof. Kai Xi, School of Chemistry, Engineering Research Center of Energy Storage Materials and Devices, Ministry of Education, National Innovation Platform (Center) for Industry-Education Integration of Energy Storage Technology, State Key Laboratory for Electrical Insulation and Power Equipment, Engineering Research Center of Energy Storage Material and Chemistry, Universities of Shaanxi Province, Xi'an Jiaotong University, Xi'an 710049, Shaanxi, China. E-mail: kx210.cam@xjtu.edu.cn; Dr. Haojie Li, College of Vehicle and Traffic Engineering, Henan University of Science and Technology, No. 48 Xiyuan Road, Jianxi District, Luoyang 471003, Henan, China. E-mail: lihaojie@haust.edu.cn; Prof. Xuetao Wang, College of Vehicle and Traffic Engineering, Henan University of Science and Technology, No. 48 Xiyuan Road, Jianxi District, Luoyang 471003, Henan, China. E-mail: wangxuetao@haust.edu.cn

**How to cite this article:** Jin, H.; Li, H.; Deng, T.; Yang, C.; Pan, K.; Jin, Z.; Zhang, Y.; Pan, S.; Ren, Y.; Li, Y.; Chen, X.; Yang, H.; Yin, S.; Wang, X.; Xi, K. Modulating carrier-catalyst heterointerfaces to boost catalytic polysulfide conversion in lithium-sulfur batteries. *Energy Mater.* 2025, 5, 500107. <https://dx.doi.org/10.20517/energymater.2025.39>

**Received:** 19 Feb 2025 **First Decision:** 19 Mar 2025 **Revised:** 25 Mar 2025 **Accepted:** 28 Mar 2025 **Published:** 19 May 2025

**Academic Editor:** Meicheng Li **Copy Editor:** Fangling Lan **Production Editor:** Fangling Lan

## Abstract

Enhancing the catalytic activity of sulfur cathode hosts is critical for suppressing the shuttle effect and accelerating the polysulfides redox kinetics in lithium-sulfur (Li-S) batteries. However, efficient polysulfide adsorption and catalysis conversion rely on synergistic interactions between the catalyst and the supporting carrier, particularly in optimizing catalytic site density and electron/ion transport rates. Herein, we modulate the carrier-catalyst



© The Author(s) 2025. **Open Access** This article is licensed under a Creative Commons Attribution 4.0 International License (<https://creativecommons.org/licenses/by/4.0/>), which permits unrestricted use, sharing, adaptation, distribution and reproduction in any medium or format, for any purpose, even commercially, as long as you give appropriate credit to the original author(s) and the source, provide a link to the Creative Commons license, and indicate if changes were made.



heterointerface to enhance polysulfide conversion. Metallic 1T-phase  $\text{MoS}_2$  nanospheres are uniformly dispersed onto the nitrogen-doped graphene (N-G) sheets, forming a composite host material (1T- $\text{MoS}_2$ /N-G) for Li-S batteries. N-G serves as both a conductive substrate for charge transfer and a support for catalyst loading, while 1T- $\text{MoS}_2$ , rich in catalytic sites, functions as an efficient electrocatalyst, promoting ion diffusion, adsorbing soluble polysulfides, and accelerating their transformation into solid lithium sulfide. Benefiting from these structural and catalytic advantages, the S/1T- $\text{MoS}_2$ /N-G cathode exhibits an initial capacity of 1,296.8 mAh  $\text{g}^{-1}$  at 0.2 C and demonstrates outstanding cycle stabilization, with a capacity decay rate of only 0.015% per cycle over 500 cycles at 1.0 C. Even under demanding conditions, such as a sulfur loading of 6.5 mg  $\text{cm}^{-2}$  and a lean electrolyte of 7  $\mu\text{L mg}^{-1}$ , the S/1T- $\text{MoS}_2$ /N-G cathode provides an initial areal capacity of 7.2 mAh  $\text{cm}^{-2}$  and retains 4.8 mAh  $\text{cm}^{-2}$  after 100 cycles. These findings offer new insights into the design of advanced catalytic materials for high-performance sulfur cathodes and broader electrocatalytic applications.

**Keywords:** Lithium-sulfur battery, 1T molybdenum disulfide, metallic phase, heterointerface modulation, polysulfides transformation

## INTRODUCTION

Lithium-sulfur (Li-S) batteries have attracted considerable attention from both academia and industry, attributable to their exceptional theoretical specific capacity (1,675 mAh  $\text{g}^{-1}$  of sulfur) and economic benefits<sup>[1-4]</sup>, positioning them as a promising alternative energy storage solution<sup>[5-7]</sup>. Nevertheless, the sluggish redox kinetics of sulfur results in the severe polysulfides shuttle effect and low sulfur utilization, primarily brought by the electronic insulation of active sulfur and discharge products ( $\text{Li}_2\text{S}_2/\text{Li}_2\text{S}$ ), as well as the complex solid-liquid-solid reactions involved<sup>[8-10]</sup>. To address these challenges, traditional carbon-based materials have been extensively utilized as hosts for the sulfur cathode, including carbon nanotubes (CNT)<sup>[11]</sup>, graphene (G)<sup>[12]</sup>, nitrogen-doped graphene (N-G)<sup>[13]</sup> and porous carbon<sup>[14]</sup>, due to their high electronic conductivity and ability to confine polysulfides. However, the insufficient interaction ability between polysulfides and carbon materials is unable to efficiently suppress polysulfides shuttling<sup>[15,16]</sup>. This becomes particularly problematic in practical applications, where high sulfur loading and lean electrolyte conditions are required, making efficient polysulfides transport difficult to achieve through simple physical or chemical adsorption in host materials alone<sup>[17,18]</sup>. Thus, host materials with highly efficient catalytic polysulfides transport capabilities have significant potential for achieving high-performance Li-S batteries<sup>[19,20]</sup>.

Transition metal compounds (TMCs) have been shown to effectively inhibit polysulfides shuttle effect through polar adsorption of polysulfides catalysis of intermediate transformations, thereby accelerating sulfur redox reaction and kinetics. Examples of such materials include oxides<sup>[21]</sup>, sulfides<sup>[22]</sup>, nitrides<sup>[23]</sup>, carbides<sup>[24]</sup> and borides<sup>[25]</sup>, which have exhibited advantages as host materials for high-performance sulfur cathodes<sup>[26,27]</sup>. Among these, the transition metal sulfides offer outstanding electrochemical advantages due to their high conductivity and increased edge active sites for catalytic intermediate reactions<sup>[28]</sup>. For instance,  $\text{MoS}_2$ <sup>[29]</sup>,  $\text{Co}_9\text{S}_8$ <sup>[30]</sup>,  $\text{VS}_2$ <sup>[31]</sup> and  $\text{ZnS}$ <sup>[32]</sup> have been confirmed improvements in polysulfides transformation kinetics. The stable chemistry of the cathode/electrolyte interface is essential for rapid charge transfer during electrocatalysis, which largely depends on the catalytically active site at the surface interface of the host material<sup>[33]</sup>. Therefore, the unique structural engineering of catalysts, particularly in regulating electron/ion transfer and polysulfides conversion, plays a critical role in achieving high-performance Li-S batteries. As a typical 2D layered structure material, there has been extensive research on the structural engineering design of  $\text{MoS}_2$  for energy storage, especially for the metallic phase 1T- $\text{MoS}_2$  with octahedral coordination structure, which has superior electrochemical advantages compared to the semiconductive 2H- $\text{MoS}_2$  with a triangular prismatic coordination mode. The high crystal symmetry of metallic phase 1T- $\text{MoS}_2$  results in an

accelerated charge transfer and more catalysis sites exposed in the electrocatalytic process, which obviously enhances the catalytic activity of 1T-MoS<sub>2</sub><sup>[34]</sup>. Currently, various catalyst design methods, including single-atom catalysts<sup>[35]</sup>, heterostructures<sup>[36]</sup> and defect engineering<sup>[37]</sup>, have been shown to improve catalytic activity for polysulfides. However, the interaction between the catalyst and its supporting carrier is often overlooked in catalyst design. The carrier typically serves as a conductive substrate that facilitates electron transfer and catalysis, contributing to enhanced catalytic activity and accelerated sulfur redox kinetics.

In this work, we modulate the carrier-catalyst interface of 1T-MoS<sub>2</sub>/N-G to enhance catalytic activity for polysulfides transformation. The flower-like 1T-phase MoS<sub>2</sub> (1T-MoS<sub>2</sub>) nanospheres are uniformly dispersed onto N-G sheets, forming a composite host material for the sulfur cathode. The metallic attributes of 1T-MoS<sub>2</sub> effectively accelerate electron/ion transfer and polysulfides transformation, thereby suppressing the shuttle effect and boosting the performance of the sulfur cathodes. As a result, S/1T-MoS<sub>2</sub>/N-G exhibits stable performance with a capacity of 845.4 mAh g<sup>-1</sup> after 500 cycles at 1 C, accompanied by a capacity decay rate of just 0.015%. Even under the sulfur loading of 6.5 mg cm<sup>-2</sup> and electrolyte usage of 7  $\mu$ L mg<sup>-1</sup>, the S/1T-MoS<sub>2</sub>/N-G cathode provides an initial capacity of 7.2 mAh cm<sup>-1</sup>, and maintains 4.8 mAh cm<sup>-1</sup> after 100 cycles. These results demonstrate a promising approach for designing host materials that enable high-capacity and stable cycling Li-S cells.

## EXPERIMENTAL

### Material preparation

All chemicals for materials preparation were analytical grade without further purification in the actual operation. The synthesis of 1T-MoS<sub>2</sub>/N-G involved two separate steps: hydrothermal treatment and annealing. Firstly, PEG-20000 (0.24 mM), N-doped graphene (4 mM), (NH<sub>4</sub>)<sub>2</sub>MoO<sub>4</sub>·2H<sub>2</sub>O (10 mM) and thioacetamide (TAA) (20 mM) were separately added to a solution containing 20 mL of deionized water and 20 mL of anhydrous ethanol, stirred and ultrasonication for 0.5 h, forming a homogenous solution. And then, the obtained medley was quickly shifted into a 60 mL stainless steel autoclave with a sustained high temperature of 200 °C for 24 h until cooled to ambient temperature, after which the solid powder deposits were washed many times with deionized water and anhydrous ethanol separately, accompanied by a subsequent 60 °C oven-baked dry processing. Secondly, the acquired product was operated in a calcination process under an Ar atmosphere at 300 °C for 2 h to yield 1T-MoS<sub>2</sub>/N-G.

For S/1T-MoS<sub>2</sub>/N-G, the typical melt-diffusion technique was employed for the composite preparation. Thus, the mixture of acquired 1T-MoS<sub>2</sub>/N-G and sulfur was continuously ground for 0.5 h with a weighting ratio of 28:72, followed by uninterrupted heating for 12 h at 155 °C in an environment filled with Ar. Yet the preparation of S/N-G was adopted to use the same technique, except for the commercial N-G employed as the host materials.

### Material characterization

Scanning electron microscopy (SEM, Hitachi FlexSEM1000) and transmission electron microscopy (TEM, JEOL-JEM-2100F) were applied to analyze the morphology and microstructure of the acquired materials. The power X-ray diffraction (XRD, BRUKER D8 Advance) was analyzed in the Cu K $\alpha$  radiation, covering a range of 5°-80°. The Raman spectra were acquired using a RENISHAW InVia Raman Spectrometer by using a 532 nm laser. Nitrogen adsorption/desorption analysis was recorded on the BELSORP MAX II apparatus. The specific surface area calculation was used by the Barret-Joyner-Halenda (BET) model, and the pore size profile calculation was used by the Barrett-Joyner-Halenda (BJH) method. Using the thermogravimetric analyzer (Mettler Toledo, TGA/DSC) to measure sulfide content with a temperature span of 30-800 °C and a heating rate of 10 °C min<sup>-1</sup>.

### Electrochemical measurements

To prepare the sulfur cathodes, the acquired composites, super P and polyvinylidene difluoride (PVDF) were mixed into N-methyl-2-pyrrolidone (NMP) respectively with a mass ratio of 8:1:1, obtaining a uniform mixture. The mixture was applied to Carbon-coated aluminum foil, then vacuum desiccated at 60 °C for 12 h, after which the electrode sheets were tailored with a 10 mm diameter for the following electrochemical test. The electrode plates of S/1T-MoS<sub>2</sub>/N-G and S/N-G with sulfur mass loading of 1.1–2 mg cm<sup>-2</sup> were measured for the general electrochemical test, and the sulfur mass loading of 6.5 mg cm<sup>-2</sup> was employed for harsh conditions with carbon cloth as the current collector. The electrochemical test was exhibited by 2032 coin-type cells assembled with Celgard 2400 as a separator and lithium foil as a reference electrode (with a diameter of 14 mm and thickness of 0.7 mm) in an argon-filled glovebox. The electrolyte consisted of 2 wt% lithium nitrate (LiNO<sub>3</sub>) with 1.0 M lithium bis(trifluoromethane sulfonimide) (LiTFSI) dissolved in 1:1 (V/V) mixture of 1,2-dimethoxyethane (DME) and 1,3-dioxolane (DOL). The electrolyte to sulfur ratio (E/S) was 10 and 7 μL mg<sup>-1</sup> for the cells with routine plates and thick plates testing, respectively. The electrochemical performance was evaluated at a voltage range of 1.7–2.8 V (vs. Li<sup>+</sup>/Li) using a LAND-CT3002A instrument. The CHI760E electrochemical workstation was used for cyclic voltammetry (CV) measurements with a voltage interval of 1.7 to 2.8 V and a fixed scan rate of 0.05–0.4 mV s<sup>-1</sup>. The PARSTAT MC electrochemical workstation was employed for measuring the electrochemical Impedance Spectra (EIS) in the frequency range of 10 mHz to 100 kHz.

### Polysulfides adsorption

All the samples were vacuum-dried at 60 °C overnight before the absorption test. Li<sub>2</sub>S<sub>6</sub> solution as the identifier of polysulfides absorption was prepared by dissolving an amount of S and Li<sub>2</sub>S (5:1) in a 1:1 (V/V) mixture of DOL and DME. The solution was vigorously stirred at 60 °C in a glovebox filled with Ar for 48 h to form a Li<sub>2</sub>S<sub>6</sub> solution (2 mM). 30 mg of the pre-processed materials 1T-MoS<sub>2</sub>/N-G or N-G were desiccated in an oven at 60 °C and introduced into 5 mL of Li<sub>2</sub>S<sub>6</sub> solution. All procedures were conducted in a glovebox filled with Ar. After soaking for 5 h, the supernatant liquid was collected for ultraviolet-visible (UV-vis) adsorption spectra measurement (QEPRO). The valence bond coordination states of the host before and after adsorption of Li<sub>2</sub>S<sub>6</sub> were measured in X-ray photoelectron spectroscopy (XPS, Thermo Fisher Scientific K-Alpha).

### Symmetric cell measurements

The symmetrical cells were assembled without sulfur in electrode and absence of lithium plates as counter electrodes. Li<sub>2</sub>S<sub>6</sub> solution of (0.2 mol L<sup>-1</sup>) was made by blending stoichiometric S and Li<sub>2</sub>S (1:5) in DOL and DME with a volume of 1:1, followed by continuous stirring to form a homogeneous solution. The symmetric cell was configured with two identical electrodes with 1T-MoS<sub>2</sub>/N-G or N-G as the working electrodes and counter electrodes. 40 μL Li<sub>2</sub>S<sub>6</sub> (0.2 mol L<sup>-1</sup>) electrolyte was dripped onto the electrode. CV was measured at a rate of 3 mV s<sup>-1</sup> from -1 to 1 V on CHI760E.

### Deposition of Li<sub>2</sub>S

Li<sub>2</sub>S<sub>8</sub> solution was used as electrolyte for lithium sulfide deposition, and 1T-MoS<sub>2</sub>/N-G or N-G was served as working electrode and lithium flake as counter electrode for cells assembled. 0.2 M Li<sub>2</sub>S<sub>8</sub> was prepared by dissolving stoichiometric S and Li<sub>2</sub>S (1:7) in tetraglyme with 1.0 M LiTFSI with continuous agitation to form a uniform solution. The blank electrolyte was made by 25 μL of Li<sub>2</sub>S<sub>8</sub> electrolyte (0.2 M) being dripped onto the work electrode, and afterwards, 25 μL of contrast electrolyte, without Li<sub>2</sub>S<sub>8</sub>, was dripped onto the counter electrode. The assembled cell was galvanostatically discharged to 2.05 V at 0.03 C, and then the potential was maintained at 2.0 V on a PARSTAT MC electrochemical workstation until the current reduction to less than 10<sup>-5</sup> A.

## RESULTS AND DISCUSSION

For achieving high-performance Li-S batteries, the innovative preparation of a cathodic host for efficient sulfur redox kinetics is designed in Figure 1. As shown in Figure 1A, although the carbon-based materials introduced polar elements such as N can inhibit shuttle effect by the pure adsorption of polysulfides, the kinetics of polysulfides conversion is still sluggish. After adjusting the carrier-catalyst heterointerface by loading metallic 1T-MoS<sub>2</sub> on the N-G [Figure 1B], the kinetics of polysulfides conversion can be obviously enhanced by the efficient catalytic activity on polysulfides and accelerated charge transfer rate via the optimized catalytic capacity and conductive properties of 1T-MoS<sub>2</sub>, which can significantly inhibit the polysulfides shuttle and facilitate the deposition of Li<sub>2</sub>S compared with the host of N-G [Figure 1C].

### Structural characterization of 1T-MoS<sub>2</sub>/N-G

To obtain 1T-MoS<sub>2</sub>/N-G host material, TAA and ammonium molybdate [(NH<sub>4</sub>)<sub>2</sub>MoO<sub>4</sub>] serve as reactants for the vulcanization and molybdenum source, respectively, as schematically shown in Supplementary Figure 1. Polyethylene glycol (PEG-20000) as a dispersant in a blended solution consisting of deionized water and anhydrous ethanol can help obtain small and dispersive molecular clusters by delaying the rate of ionic hydrolysis, while N-G [Figure 2A] provides dispersed support sites and a conductive skeleton for the synthesized MoS<sub>2</sub> in the hydrothermal reaction. The subsequent annealing in argon (Ar) atmosphere contributes to improving the crystallinity of 1T phase molybdenum disulfide, and 1T-MoS<sub>2</sub>/N-G preparation is completed.

As illustrated in Figure 2B and Supplementary Figure 2, the nanospheres composed of flower-like 1T-MoS<sub>2</sub> nanosheets are uniformly dispersed on N-G, and have a size of ~500 nm. The element distribution predicted by energy-dispersion spectroscopy (EDS) of 1T-MoS<sub>2</sub>/N-G [Figure 2C] verifies that MoS<sub>2</sub> is successfully synthesized and the load is uniformly dispersed on N-G. The crystal phase structure analysis of 1T-MoS<sub>2</sub>/N-G was further performed with TEM. The flower-like structures are further verified in Figure 2D. Upon the high-resolution TEM (HRTEM) picture in Figure 2E, in which the crystal spacing of 0.476 nm and the inserted Fast Fourier Transform (FFT) pattern correspond to the new (004) plane of 1T-MoS<sub>2</sub>. Especially, the Inverse FFT (IFFT) consequence corresponding to the boxed area in Figure 2E shows a characteristic atomic distribution of 1T-MoS<sub>2</sub> [Figure 2F]. In addition, the lattice fringe arrangement [Figure 2G] shows a regular distribution of atoms in the crystalline structure of 1T-MoS<sub>2</sub>.

The XRD patterns of 1T-MoS<sub>2</sub>/N-G and N-G [Figure 2H, Supplementary Figure 3] indicate new crystal faces (002) and (004) of 1T-MoS<sub>2</sub><sup>[38]</sup>, which are in agreement with the result of the HRTEM picture in Figure 2E. Furthermore, the Raman spectrum in Figure 2I shows characteristic vibration mode peaks at 143.3 cm<sup>-1</sup> (*J*<sub>1</sub>), 234.7 cm<sup>-1</sup> (*J*<sub>2</sub>), 278.9 cm<sup>-1</sup> (*E*<sub>1g</sub>) and 334.7 cm<sup>-1</sup> (*J*<sub>3</sub>), which corresponds to the typical modes of 1T-MoS<sub>2</sub> crystalline phase<sup>[39,40]</sup>. N<sub>2</sub> adsorption-desorption isotherms are tested for the specific surface area and pore size profile of 1T-MoS<sub>2</sub>/N-G and N-G. The results [Figure 2J, Supplementary Figure 4, Supplementary Table 1] show that 1T-MoS<sub>2</sub>/N-G has a specific surface area of 307.16 m<sup>2</sup> g<sup>-1</sup> and an average pore of 4.54 nm, respectively.

### Effect of 1T-MoS<sub>2</sub> on catalytic performance

The electrocatalytic transmission of soluble intermediate polysulfides is a critical factor in the continuous transformation of diffusion, adsorption, and charge-transfer process, which can ensure efficient sulfur utilization in the cathode<sup>[41]</sup>. For electrocatalytic process, the effective adsorption between base material and polysulfides plays a vital role in front of the subsequent catalytic conversion process. Firstly, the static adsorption experiments were employed to detect the adsorption performance for polysulfides by immersing 1T-MoS<sub>2</sub>/N-G or N-G into Li<sub>2</sub>S<sub>6</sub> solution. After 5 h, the supernatant was gained and analyzed using a UV-



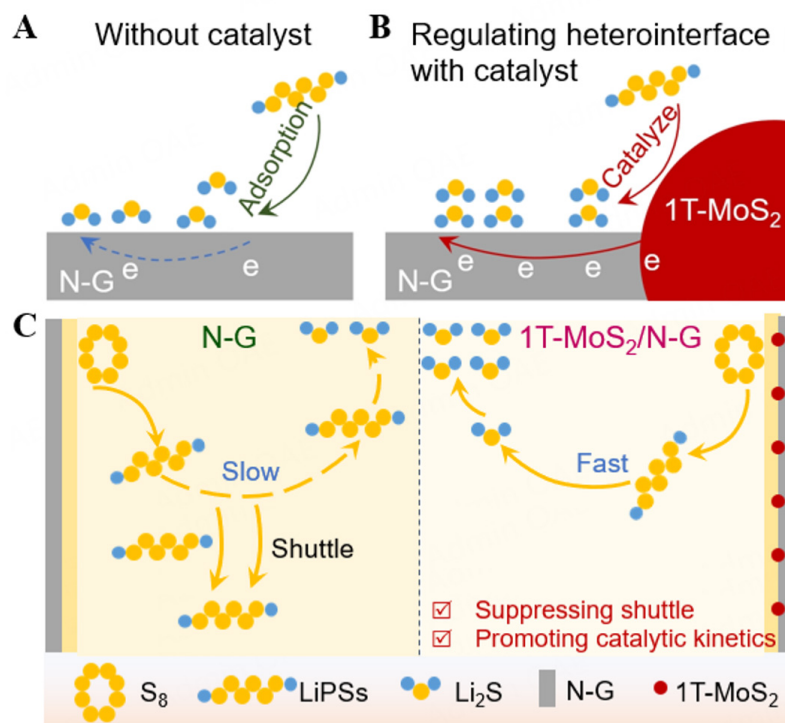


**Figure 1.** Regulating the sulfur conversion mechanism based on sulfur-host materials; (A) Carrier without catalytic active sites; (B) Modulated heterointerface of carrier-catalyst with catalyst; (C) Details of polysulfide conversion mechanism on N-G and 1T-MoS<sub>2</sub>/N-G hosts, respectively.

Vis spectrophotometer [Figure 3A]. The colorless liquid after interaction with Li<sub>2</sub>S<sub>6</sub> and a weak absorption peak in the UV-Vis spectra indicate that 1T-MoS<sub>2</sub> can effectively strengthen the adsorption capacity of polysulfides. The bonding states and valence of 1T-MoS<sub>2</sub>/N-G before and after adsorption of Li<sub>2</sub>S<sub>6</sub> were analyzed by XPS. In the high-resolution spectra of the Mo 3d orbit (Figure 3B, before adsorption of Li<sub>2</sub>S<sub>6</sub>), the strong peaks at 228.5 (Mo 3d<sub>5/2</sub>) and 231.6 eV (Mo 3d<sub>3/2</sub>) correspond to Mo<sup>4+</sup> (1T-MoS<sub>2</sub>), and the weaker peaks at 225.9 and 234.8 eV correspond to the peak binding energy of S 2s and Mo<sup>6+</sup>, respectively. After the interaction with Li<sub>2</sub>S<sub>6</sub>, the XPS spectral characteristic peak of the Mo 3d orbital negatively shifts to lower binding energy, which can be attributed to the electron transfer from Li<sub>2</sub>S<sub>6</sub> to the Mo atoms. In addition, the peaks located at 161.5 and 162.9 eV separately belong to terminal (ST<sup>-1</sup>) and bridging sulfur (SB<sup>0</sup>) atoms in the S 2p of 1T-MoS<sub>2</sub>/N-G-Li<sub>2</sub>S<sub>6</sub>, which are obviously shift to lower binding energy compared with the S 2p of proto-Li<sub>2</sub>S<sub>6</sub> ST<sup>-1</sup> (161.7 eV) and SB<sup>0</sup> (163.1 eV), respectively<sup>[42]</sup> [Figure 3C]. The negative shift of the S 2p spectral peak in 1T-MoS<sub>2</sub>/N-G-Li<sub>2</sub>S<sub>6</sub> indicates a chemical interaction between the polysulfide and 1T-MoS<sub>2</sub>. Secondly, the catalytic dynamic of 1T-MoS<sub>2</sub> to polysulfides was investigated; the symmetric cells were assembled with 1T-MoS<sub>2</sub>/N-G and N-G as catalytic cathodes. Electrochemical impedance spectroscopy (EIS) in Figure 3D shows that the smaller interface charge transfer resistance ( $R_{ct}$ ) of 1T-MoS<sub>2</sub>/N-G (Supplementary Table 2, fitted equivalent circuit in Supplementary Figure 5) indicates a faster charge transfer rate than N-G, which is ascribed to the profitable conductivity of metallic 1T-MoS<sub>2</sub>. Furthermore, the exchange current density  $j_0$  of a catalytic electrode [Figure 3E] is calculated by the subsequent Equation (1)<sup>[43]</sup>

$$j_0 = RT/nFR_{ct} \quad (1)$$

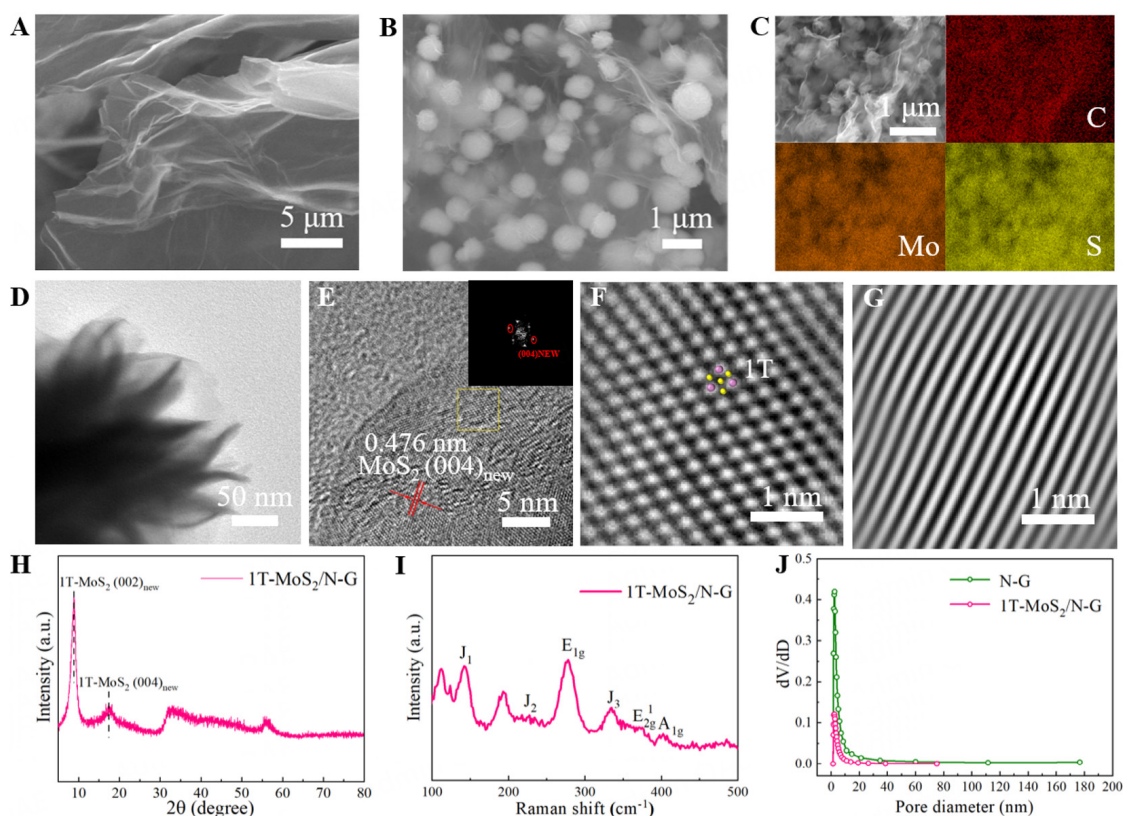


**Figure 2.** SEM pictures of (A) N-G and (B) 1T-MoS<sub>2</sub>/N-G; (C) EDS elemental mapping of 1T-MoS<sub>2</sub>/N-G; (D) TEM and (E) HRTEM pictures of 1T-MoS<sub>2</sub>/N-G [(E), inserted the corresponding FFT patterns]; The IFFT patterns of (F) Lattice profiles and (G) Lattice spacing profiles, respectively (based on the yellow boxed area in HRTEM picture (E); (F), in the covered atomic configurations, purple dot represents molybdenum atom, yellow dot represents sulfur atom); (H) XRD pattern and (I) Raman spectrum of 1T-MoS<sub>2</sub>/N-G; (J) The pore size distribution of 1T-MoS<sub>2</sub>/N-G and N-G.

where  $R$ ,  $T$ ,  $n$  and  $F$  represent gas content, absolute temperature, number of elements being transferred and Faraday content, respectively, and  $R_{ct}$  is charge transfer impedance from Figure 3D, Supplementary Table 2. The optimized exchange current density of 1T-MoS<sub>2</sub>/N-G exhibits a faster charge transfer from the electrode reaction compared to N-G. In addition, the CV curves of the symmetric cell deliver a significantly high current response of 1T-MoS<sub>2</sub>/N-G, thus demonstrating an efficient catalytic activity for polysulfides conversion<sup>[44]</sup> [Figure 3F], which is well matched with the results of  $j_0$ .

Due to the continuous conversion reactions of dissolution-deposition mechanism of sulfur cathode, the catalytic efficiency of polysulfides mainly depends on the conversion capacity from soluble Li<sub>2</sub>S<sub>x</sub> to Li<sub>2</sub>S<sub>2</sub> and Li<sub>2</sub>S<sup>[45]</sup>. To further examine how catalysts regulate the nucleation and growth of solid discharge products, the Li<sub>2</sub>S deposition experiment was carried out. As we can see in Figure 3G and H, the Li<sub>2</sub>S deposition amount on 1T-MoS<sub>2</sub>/N-G substrate is obviously larger and the response time is shorter than N-G, which has a consistent trend with the EIS analysis, indicating a diminished energy barrier for Li<sub>2</sub>S deposition on 1T-MoS<sub>2</sub> substrate surface. Thus, the calculated Li<sub>2</sub>S deposition capacity for 1T-MoS<sub>2</sub>/N-G is 298.1 mAh g<sup>-1</sup> based on Faraday's law<sup>[46]</sup>, which is higher than that of N-G (96.9 mAh g<sup>-1</sup>), showing a stronger redox kinetics to catalyze polysulfides to Li<sub>2</sub>S.

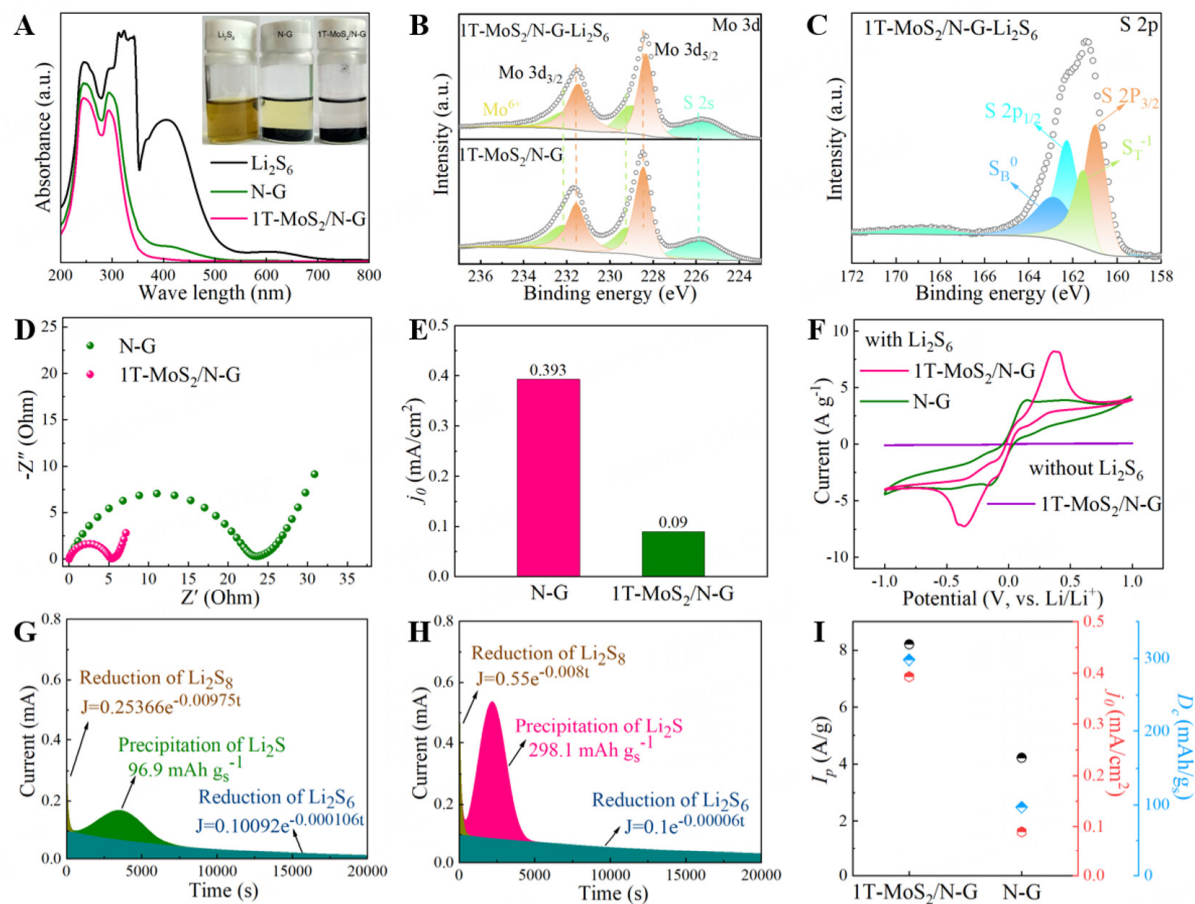


**Figure 3.** (A) Visualization of the adsorption effect of Li<sub>2</sub>S<sub>6</sub> by 1T-MoS<sub>2</sub>/N-G and N-G after 5 h submersion and the supernatants for UV-vis test; XPS spectra of (B) Mo 3d and (C) S 2p on interaction of 1T-MoS<sub>2</sub>/N-G with Li<sub>2</sub>S<sub>6</sub>; (D) EIS spectra and (E) exchange current density measured by symmetric cells with Li<sub>2</sub>S<sub>6</sub> solution of 1T-MoS<sub>2</sub>/N-G and N-G; (F) CV curves measured by symmetric cells with Li<sub>2</sub>S<sub>6</sub> solution of 1T-MoS<sub>2</sub>/N-G and N-G; (G and H) Galvanostatic discharged curves using Li<sub>2</sub>S<sub>6</sub>/tetraglyme electrolyte at 2.0 V based on 1T-MoS<sub>2</sub>/N-G and N-G electrode; (I) Comparison of comprehensive performance based on electrochemical testing from (D-H).

Based on the above electrochemical analysis, the comprehensive electrochemical performance of the 1T-MoS<sub>2</sub>/N-G host materials can be quantitatively assessed. Also, the  $D_c$  reflects the amount of Li<sub>2</sub>S deposition, the peak current density  $I_p$  of the CV curve corresponds to ionic diffusion rate at the substrate interface and the exchange current density  $j_0$  of catalytic electrode demonstrates the sulfur electrode reaction kinetics. Therefore,  $D_c$ ,  $j_0$ , and  $I_p$  are summarized in Figure 3I for synthetic comparison. Obviously, the catalytic capacity of 1T-MoS<sub>2</sub>/N-G is stronger, resulting in improved redox kinetics for polysulfides intermediate transformation.

### Characterization of structure and electrochemical performance of S/1T-MoS<sub>2</sub>/N-G and S/N-G

The S/1T-MoS<sub>2</sub>/N-G and S/N-G were synthesized by the classical molten diffusion strategy<sup>[47]</sup>. The SEM images in Supplementary Figure 6 show that the sulfur is uniformly loaded on the host material, and the overall structure morphology after merging sulfur remains basically unchanged, indicating a dense recombination with sulfur. Moreover, XRD pattern [Supplementary Figure 7A] reveals that sulfur exists in the composite as the monoclinic phase<sup>[48]</sup>, and the sulfur content of the two composites is basically maintained at ~72 wt% on the basis of thermogravimetric results (TGA) in Supplementary Figure 7B. The specific surface area and pore size profile of 1T-MoS<sub>2</sub>/N-G and N-G after sulfur melting



[Supplementary Figure 8, Supplementary Table 1] show an obviously decreased trend, indicating the well-filled sulfur within the interface and pores of the host materials.

Furthermore, S/1T-MoS<sub>2</sub>/N-G and S/N-G were used to assemble the Li-S batteries for electrochemical testing. Figure 4A showcases the typical CV curves of Li-S batteries<sup>[49]</sup> using S/1T-MoS<sub>2</sub>/N-G and S/N-G as sulfur cathodes. Compared to S/N-G, S/1T-MoS<sub>2</sub>/N-G exhibits a reinforced peak current and a sharper peak shape in the cathodic/anodic reaction [Supplementary Figure 9]. Especially, the CV peak of S/1T-MoS<sub>2</sub>/N-G battery has less overpotential in the redox electrochemical process [Figure 4B]. The Tafel curves were applied to further assess the electrocatalytic properties of 1T-MoS<sub>2</sub> during redox reaction. Tafel slope is used to describe the polarization of the electrode based on the relationship between overpotential and current density during electrochemical reaction. The smaller value reveals an accelerated electrode response and enhanced electrochemical kinetics. In Li-S batteries, the smaller Tafel slope verifies a strong dynamic in sulfur redox reaction and an efficient catalytic polysulfide conversion<sup>[50]</sup>. As displayed in Figure 4C-E, the fitting slopes of peaks a, b, and c for S/1T-MoS<sub>2</sub>/N-G cell are 44.79, 25.24 and 40.85 mV dec<sup>-1</sup>, respectively, which are distinctly lower than S/N-G cell (46.26, 42.57, 49.73 mV dec<sup>-1</sup>, respectively), indicating an accelerated polysulfides redox kinetics than S/N-G. The consistent electrochemical property is also demonstrated by EIS test in Figure 4F. Comparing the fitting circuit element data analysis in Supplementary Table 3, the Li-S battery assembled by S/1T-MoS<sub>2</sub>/N-G cathode exhibits a smaller charge transfer impedance  $R_{ct}$  (32.73  $\Omega$ ), which is lower than that of S/N-G (96.94  $\Omega$ ). The higher exchange current density of S/1T-MoS<sub>2</sub>/N-G ( $6.25 \times 10^{-2}$  mA cm<sup>-2</sup>) calculated by Equation (1) proves the enhanced kinetics of polysulfides ion transport in the electrochemical cycle than S/N-G ( $2.11 \times 10^{-2}$  mA cm<sup>-2</sup>) [Supplementary Figure 10], which matches with the results of Figure 3D. This can be attributed to the metallic 1T-MoS<sub>2</sub> and optimized heterointerfaces of 1T-MoS<sub>2</sub> and N-G. On the one hand, the metallic 1T-MoS<sub>2</sub> interaction with polysulfide can accelerate the electron transfer in adsorption and catalytic polysulfide conversion to enhance the reaction rate of sulfur redox, which can efficiently decrease the charge transfer resistance. On the other hand, the heterointerfaces modulated by catalysis 1T-MoS<sub>2</sub> loaded on N-G can optimize the adsorption-catalysis functional region to reduce the interface resistance and improve the reaction kinetics of sulfur electrodes. In addition, lithium-ion diffusion coefficient was investigated by the CV tests with different sweep speeds from 0.05 to 0.4 mV s<sup>-1</sup>. As shown in Figure 4G and Supplementary Figure 11A, the peak current of CV curves in S/1T-MoS<sub>2</sub>/N-G and S/N-G cathodes is enhanced gradually, which positively corresponds to the scan rate of the CV test. Besides, the current of anodic and cathodic peaks is linearly correlated with the square root of the sweep speed based on the Randles-Sevcik equation<sup>[51]</sup>, which is consistent with previous reports<sup>[52,53]</sup>. The slope  $I_p/v^{0.5}$  reflects the lithium-ion diffusion rate defined by peak current  $I_p$  and square root of scanning speed of  $v$ . Thus, the Li<sup>+</sup> diffusion rate of S/1T-MoS<sub>2</sub>/N-G [Figure 4H and I] is higher than that of the S/N-G cathode [Supplementary Figure 11B and C], proving improved redox kinetics and electrocatalytic reaction on the S/1T-MoS<sub>2</sub>/N-G cathode surface.

The batteries with S/1T-MoS<sub>2</sub>/N-G and S/N-G as the cathode were used to estimate the cyclic performance in Figure 5. The capacity contribution of 1T-MoS<sub>2</sub>/N-G is negligible [Supplementary Figure 12A and B] in the voltage interval of Li-S batteries (1.7–2.8 V vs. Li<sup>+</sup>/Li). The initial charge-discharge plateaus of S/1T-MoS<sub>2</sub>/N-G [Figure 5A] show a typical multistep discharge profile and deliver a higher discharge capacity of 1,296.8 mAh g<sup>-1</sup> at 0.2 C, which is higher than S/N-G (1,002.1 mAh g<sup>-1</sup>). Besides, the overpotential of S/1T-MoS<sub>2</sub>/N-G is significantly smaller (0.172 V) than that of S/N-G cathode (0.204 V, in Supplementary Figure 13), which is evaluated by the difference of median potential at the intermediate point of discharge capacity from the vertical corresponding of charge curve<sup>[54]</sup>, and the slight voltage jump of S/1T-MoS<sub>2</sub>/N-G (~2.295 V) shows a lower activation energy barrier than S/N-G (~2.329 V) [Figure 5B],

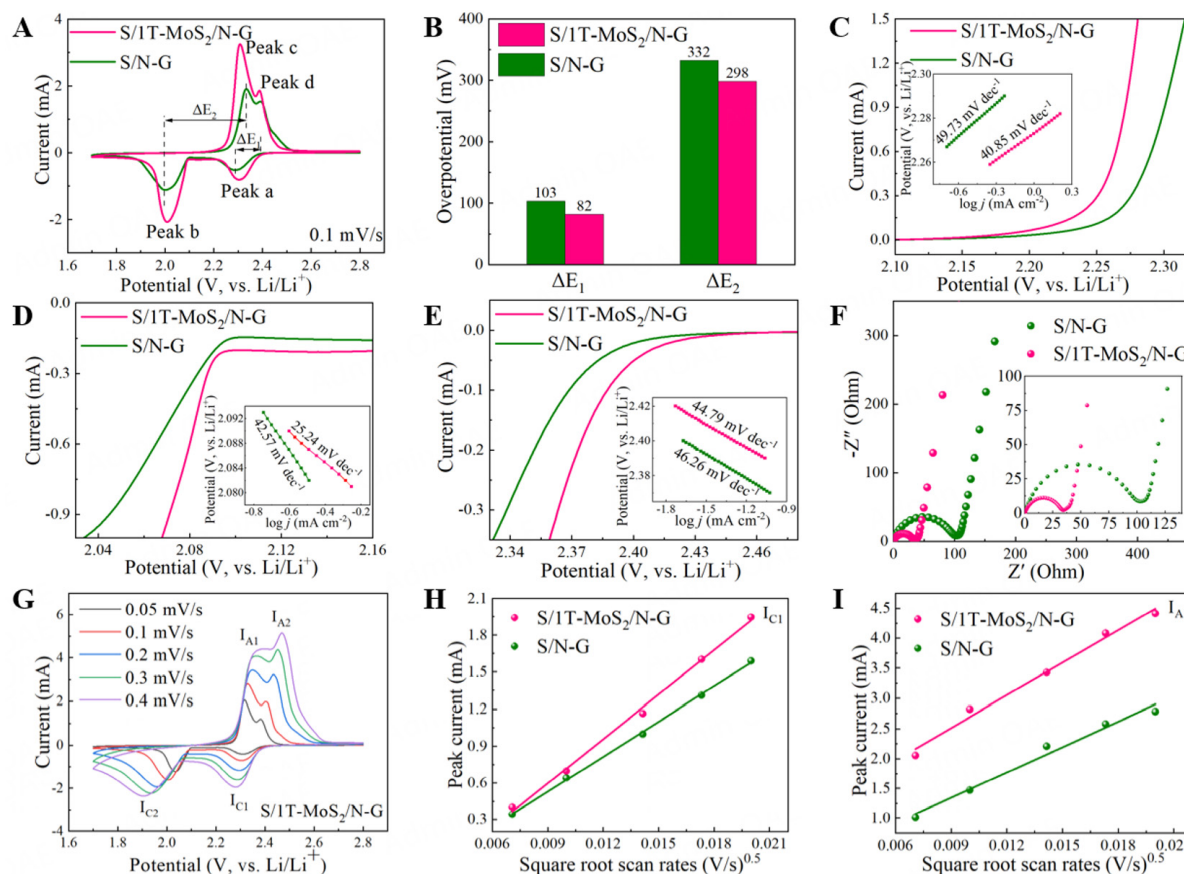


**Figure 4.** (A) CV curves of S/1T-MoS<sub>2</sub>/N-G and S/N-G cathodes with a scan rate of 0.1 mV s<sup>-1</sup> and (B) overpotential diagram; Tafel plots of (C) peak c, (D) peak b, and (E) peak a based on the CV curves of (A); (F) EIS spectra of S/1T-MoS<sub>2</sub>/N-G and S/N-G cathodes before cycle; (G) CV curves of S/1T-MoS<sub>2</sub>/N-G at the different scan rate from 0.05 to 0.4 mV s<sup>-1</sup>, and (H and I) the relationships between the peak current and scan rate for different reaction processes based on (G).

indicating a faster solid-liquid phase conversion from Li<sub>2</sub>S to polysulfides<sup>[48]</sup>. When it cycled for 200 cycles, the S/1T-MoS<sub>2</sub>/N-G cathode maintains a discharge capacity of 997 mAh g<sup>-1</sup> and a coulomb efficiency of 99.77%, showing a higher capacity retention than S/N-G (Figure 5C, capacity of 588.7 mAh g<sup>-1</sup>, coulomb efficiency of 97.22%). Also, S/1T-MoS<sub>2</sub>/N-G exhibits a terrific rate capacity. As showcased in Figure 5D, the average discharge specific capacity of S/1T-MoS<sub>2</sub>/N-G can separately maintain 1,257.28, 1,153.66, 1,045.68, 968.08 and 890.94 mAh g<sup>-1</sup> with a current density of 0.1, 0.2, 0.5, 1 and 2 C, which obviously contrast with S/N-G having a lesser capacity at different current density, especially for 2 C rate, only 230 mAh g<sup>-1</sup> accomplished. The charge-discharge platforms of S/1T-MoS<sub>2</sub>/N-G reveal smaller overpotential at different cycled rates than that of S/N-G and the gap gradually increased with the current density [Figure 5E and Supplementary Figure 14], closely similar to the results of Figure 5A. When the current density soars to 2 C, a typical multistep discharge profile of S/1T-MoS<sub>2</sub>/N-G can be maintained, in contrast with a sharp capacity drop of S/N-G and the 2nd discharge plateau almost disappearing, showing an improved electrochemical performance by the effect of 1T-MoS<sub>2</sub>/N-G cathode.

Furthermore, S/1T-MoS<sub>2</sub>/N-G cathodes can also achieve superior electrochemical performance with harsh conditions of high sulfur loading and low E/S (electrolyte/sulfur ratio) for practical inquiry. The typical multistep discharge profile of S/1T-MoS<sub>2</sub>/N-G can be maintained with a slight decrease in discharge potential. Thus, the initial discharge capacity can reach 1,108 mAh g<sup>-1</sup> with a sulfur loading of 6.5 mg cm<sup>-2</sup>

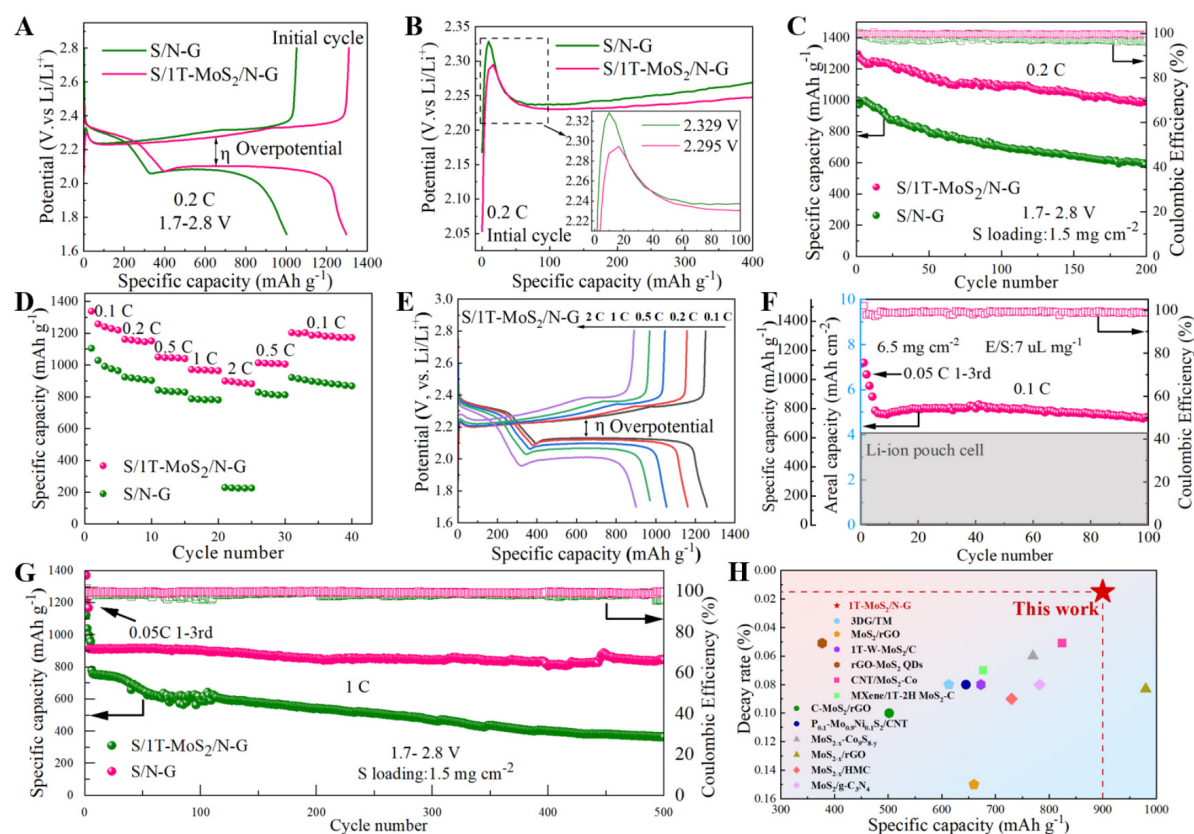


**Figure 5.** (A) The initial charge-discharge plateaus of S/1T-MoS<sub>2</sub>/N-G and S/N-G electrodes at 0.2 C and (B) corresponding enlarged view; (C) Cycling performance at 0.2 C; (D) Valuation of the multiplicity cycles and (E) charge-discharge plateaus of S/1T-MoS<sub>2</sub>/N-G cathode; (F) Cycling performance with highly sulfur loading and lean electrolyte/sulfur ratio; (G) Long cycling performances at 1 C; (H) Comprehensive performance comparison diagram.

and electrolyte usage of 7  $\mu\text{L mg}^{-1}$ , accompanying a slight platform drop [Supplementary Figure 15]. Besides, the area capacity still maintains 4.8 mAh cm<sup>-2</sup> (739 mAh g<sup>-1</sup>) after cycling 100 times with a current density of 0.1 C (1-3rd at 0.05 C for activation), which is observably superior to that of commercialized lithium-ion batteries (LIBs, 4.0 mAh cm<sup>-2</sup>) [Figure 5F] and competitive for capacity retention compared with the MoS<sub>2</sub> related host materials under high sulfur loading and low electrolyte usage [Supplementary Table 4]. At the same time, S/1T-MoS<sub>2</sub>/N-G cathodes also show excellent long-cycle stability, maintaining a discharge capacity of 845.4 mAh g<sup>-1</sup> after 500 cycles, and have an exceptionally low-capacity decay rate of 0.015% per cycle (based on the 4th cycle) [Figure 5G]. In contrast, the S/N-G only reaches a capacity of 365.6 mAh g<sup>-1</sup> after cycling 500 times with a larger capacity decay of 0.107%. Compared with molybdenum disulfide-related host materials in recent years, S/1T-MoS<sub>2</sub>/N-G of this work is encouraging for Li-S batteries [Figure 5H and Supplementary Table 5].

The crystal phase structure of 1T-MoS<sub>2</sub> can be stably maintained in the charging and discharging cycle. After cycling 200 times at 0.2 C, the S/1T-MoS<sub>2</sub>/N-G cathode was characterized by TEM. As revealed in Supplementary Figure 16, the cycled electrodes show a typical 2D sheet stack morphology [Supplementary Figure 16A], and the new (004) plane of 1T-MoS<sub>2</sub> corresponding to the 0.476 nm interplanar spacing can still be clearly displayed in HRTEM [Supplementary Figure 16B]. Furthermore, the IFFT results [Supplementary Figure 16C and D] also show the characteristic atomic distribution and lattice fringe of 1T-MoS<sub>2</sub>. So, the results strongly prove that the 1T-MoS<sub>2</sub> crystal phase structure is relatively stable

during the charge-discharge cycle and has a sustained and efficient catalytic effect on polysulfides conversion in Li-S batteries.

## CONCLUSIONS

In summary, by modulating the carrier-catalyst heterointerfaces, the kinetics of polysulfides transformation in the sulfur cathode are significantly enhanced. The metallic 1T-MoS<sub>2</sub> phase, featuring a nanoflower structure, is successfully incorporated into the sulfur cathode, resulting in high-performance Li-S batteries. The metallic 1T-MoS<sub>2</sub>, composed of numerous nanosheets, provides efficient conductivity for electron and ion transport. Additionally, 1T-MoS<sub>2</sub> loaded on N-G not only effectively chemisorbs intermediate polysulfides but also accelerates the interconversion of soluble lithium polysulfides and solid Li<sub>2</sub>S<sub>2</sub>/Li<sub>2</sub>S, thereby improving the sulfur redox kinetics. Benefiting from the superb catalytic activity of 1T-MoS<sub>2</sub>, the S/1T-MoS<sub>2</sub>/N-G cathode exhibits a satisfactory initial areal capacity of 7.2 mAh cm<sup>-1</sup> under a sulfur load of 6.5 mg cm<sup>-2</sup> and outstanding stable cycling with a decay rate of 0.015% over 500 cycles at 1 C. This work furnishes valuable insights for designing and fabricating efficient, multifunctional catalytic TMCs host materials for high-performance Li-S batteries.

## DECLARATIONS

### Authors' contributions

Experimentation: Jin, H.

Investigation, methodology: Jin, H.; Deng, T.; Jin, Z.; Zhang, Y.

Materials characterization: Jin, H.; Yang, C.; Ren, Y.; Li, Y.; Chen, X.; Yang, H.

Data analysis: Jin, H.; Li, H.; Yang, C.; Pan, S.; Yin, S.

Conceptualization and supervision: Li, H.; Wang, X.; Pan, K.

Writing-original draft: Jin, H.; Li, H.; Xi, K.; Yang, C.

Review and editing: Li, H.; Xi, K.

### Availability of data and materials

The data are available upon request from the authors.

### Financial support and sponsorship

This work was supported by the National Energy Storage Platform, Key Technologies R & D Program of Henan Province (232102240009, 252102240069), Major Science and Technology Projects of Henan Province (241100240400), Major Scientific and Technological Innovation Project in Henan Province (231100220100), Longmen Laboratory Free Exploration Project (LMQYTSKT012, LMQYTSKT015) and Natural Science Foundation Project of Henan Province (232300420087), the National Natural Science Foundation of China (No. 92472124 and No. 22278329).

### Conflicts of interest

All authors declared that there are no conflicts of interest.

### Ethical approval and consent to participate

Not applicable.

### Consent for publication

Not applicable.



## Copyright

© The Author(s) 2025.

## REFERENCES

1. Wang, P.; Xi, B.; Huang, M.; Chen, W.; Feng, J.; Xiong, S. Emerging catalysts to promote kinetics of lithium-sulfur batteries. *Adv. Energy. Mater.* **2021**, *11*, 2002893. DOI
2. Chung, S. H.; Manthiram, A. Current status and future prospects of metal-sulfur batteries. *Adv. Mater.* **2019**, *31*, e1901125. DOI PubMed
3. Evers, S.; Nazar, L. F. New approaches for high energy density lithium-sulfur battery cathodes. *Acc. Chem. Res.* **2013**, *46*, 1135-43. DOI PubMed
4. Xia, S.; Xu, X.; Wu, W.; et al. Advancements in functionalized high-performance separators for lithium-sulfur batteries. *Mater. Sci. Eng. R. Rep.* **2025**, *163*, 100924. DOI
5. Kamaya, N.; Homma, K.; Yamakawa, Y.; et al. A lithium superionic conductor. *Nat. Mater.* **2011**, *10*, 682-6. DOI
6. Wang, J.; Li, G.; Luo, D.; et al. Engineering the conductive network of metal oxide-based sulfur cathode toward efficient and longevous lithium-sulfur batteries. *Adv. Energy. Mater.* **2020**, *10*, 2002076. DOI
7. He, X.; Bresser, D.; Passerini, S.; et al. The passivity of lithium electrodes in liquid electrolytes for secondary batteries. *Nat. Rev. Mater.* **2021**, *6*, 1036-52. DOI
8. Guo, Y.; Niu, Q.; Pei, F.; et al. Interface engineering toward stable lithium-sulfur batteries. *Energy. Environ. Sci.* **2024**, *17*, 1330-67. DOI
9. Qu, Z.; Zhang, X.; Xiao, R.; Sun, Z.; Li, F. Application of organosulfur compounds in lithium-sulfur batteries. *Acta. Phys. Chim. Sin.* **2023**, *39*, 2301019. DOI
10. Bi, C. X.; Yao, N.; Li, X. Y.; et al. Unveiling the reaction mystery between lithium polysulfides and lithium metal anode in lithium-sulfur batteries. *Adv. Mater.* **2024**, *36*, e2411197. DOI
11. Cheng, X.; Huang, J.; Zhang, Q.; Peng, H.; Zhao, M.; Wei, F. Aligned carbon nanotube/sulfur composite cathodes with high sulfur content for lithium-sulfur batteries. *Nano. Energy.* **2014**, *4*, 65-72. DOI
12. Fang, R.; Chen, K.; Yin, L.; Sun, Z.; Li, F.; Cheng, H. M. The regulating role of carbon nanotubes and graphene in lithium-ion and lithium-sulfur batteries. *Adv. Mater.* **2019**, *31*, e1800863. DOI
13. Qiu, Y.; Li, W.; Zhao, W.; et al. High-rate, ultralong cycle-life lithium/sulfur batteries enabled by nitrogen-doped graphene. *Nano. Lett.* **2014**, *14*, 4821-7. DOI
14. Li, G.; Sun, J.; Hou, W.; Jiang, S.; Huang, Y.; Geng, J. Three-dimensional porous carbon composites containing high sulfur nanoparticle content for high-performance lithium-sulfur batteries. *Nat. Commun.* **2016**, *7*, 10601. DOI PubMed PMC
15. Zhou, G.; Chen, H.; Cui, Y. Formulating energy density for designing practical lithium-sulfur batteries. *Nat. Energy.* **2022**, *7*, 312-9. DOI
16. Li, J.; Gao, L.; Pan, F.; et al. Engineering strategies for suppressing the shuttle effect in lithium-sulfur batteries. *Nanomicro. Lett.* **2023**, *16*, 12. DOI PubMed PMC
17. Li, S.; Wang, W.; Duan, H.; Guo, Y. Recent progress on confinement of polysulfides through physical and chemical methods. *J. Energy. Chem.* **2018**, *27*, 1555-65. DOI
18. Lian, Z.; Ma, L.; Wu, H.; et al. Accelerating sulfur redox kinetics by rare earth single-atom electrocatalysts toward efficient lithium-sulfur batteries. *Appl. Catal. B. Environ. Energy.* **2025**, *361*, 124661. DOI
19. Huang, Y.; Lin, L.; Zhang, C.; et al. Recent advances and strategies toward polysulfides shuttle inhibition for high-performance Li-S batteries. *Adv. Sci.* **2022**, *9*, e2106004. DOI PubMed PMC
20. Wang, P.; Xi, B.; Xiong, S. Insights into the optimization of catalytic active sites in lithium-sulfur batteries. *Acc. Chem. Res.* **2024**, *57*, 2093-104. DOI
21. Wang, B.; Ren, Y.; Zhu, Y.; et al. Construction of Co<sub>3</sub>O<sub>4</sub>/ZnO heterojunctions in hollow N-doped carbon nanocages as microreactors for lithium-sulfur full batteries. *Adv. Sci.* **2023**, *10*, e2300860. DOI PubMed PMC
22. Liu, L.; Yan, M.; Zhao, X.; Pan, H. A novel pathway for sustained sulfides conversion via electrocatalyst-modified separator in lithium-sulfur batteries. *Nano. Energy.* **2024**, *130*, 110122. DOI
23. Yang, M.; Liu, P.; Qu, Z.; et al. Nitrogen-vacancy-regulated Mo<sub>2</sub>N quantum dots electrocatalyst enables fast polysulfides redox for high-energy-density lithium-sulfur batteries. *Nano. Energy.* **2022**, *104*, 107922. DOI
24. Yuan, H.; Zheng, J.; Lu, G.; et al. Formation of 2D amorphous lithium sulfide enabled by Mo<sub>2</sub>C clusters loaded carbon scaffold for high-performance lithium sulfur batteries. *Adv. Mater.* **2024**, *36*, e2400639. DOI
25. He, J.; Bhargava, A.; Manthiram, A. Molybdenum boride as an efficient catalyst for polysulfide redox to enable high-energy-density lithium-sulfur batteries. *Adv. Mater.* **2020**, *32*, e2004741. DOI
26. Chen, L.; Cao, G.; Li, Y.; et al. A review on engineering transition metal compound catalysts to accelerate the redox kinetics of sulfur cathodes for lithium-sulfur batteries. *Nanomicro. Lett.* **2024**, *16*, 97. DOI PubMed PMC
27. Pan, H.; Cheng, Z.; Zhou, Z.; et al. Boosting lean electrolyte lithium-sulfur battery performance with transition metals: a comprehensive review. *Nanomicro. Lett.* **2023**, *15*, 165. DOI PubMed PMC
28. Wu, J.; Ye, T.; Wang, Y.; et al. Understanding the catalytic kinetics of polysulfide redox reactions on transition metal compounds in



- Li-S batteries. *ACS. Nano.* **2022**, 16, 15734-59. DOI
29. Zhang, J.; Xie, Z.; Xi, W.; et al. 3D printing of tungstate anion modulated 1T-MoS<sub>2</sub> composite cathodes for high-performance lithium-sulfur batteries. *Adv. Energy. Mater.* **2024**, 14, 2401792. DOI
  30. Li, H.; Song, Y.; Xi, K.; et al. Sulfur vacancies in Co<sub>9</sub>S<sub>8-x</sub>/N-doped graphene enhancing the electrochemical kinetics for high-performance lithium-sulfur batteries. *J. Mater. Chem. A.* **2021**, 9, 10704-13. DOI
  31. Liu, G.; Zeng, Q.; Fan, Z.; et al. Boosting sulfur catalytic kinetics by defect engineering of vanadium disulfide for high-performance lithium-sulfur batteries. *Chem. Eng. J.* **2022**, 448, 137683. DOI
  32. Wang, J.; Zhao, Y.; Li, G.; et al. Aligned sulfur-deficient ZnS<sub>1-x</sub> nanotube arrays as efficient catalyzer for high-performance lithium/sulfur batteries. *Nano. Energy.* **2021**, 84, 105891. DOI
  33. Zhong, Y.; Yin, L.; He, P.; Liu, W.; Wu, Z.; Wang, H. Surface chemistry in cobalt phosphide-stabilized lithium-sulfur batteries. *J. Am. Chem. Soc.* **2018**, 140, 1455-9. DOI
  34. Chen, X.; Wang, Z.; Wei, Y.; et al. High phase-purity 1T-MoS<sub>2</sub> ultrathin nanosheets by a spatially confined template. *Angew. Chem. Int. Ed.* **2019**, 58, 17621-4. DOI
  35. Wang, J.; Cao, G.; Duan, R.; Li, X.; Li, X. Advances in single metal atom catalysts enhancing kinetics of sulfur cathode. *Acta. Phys. Chim. Sin.* **2023**, 39, 2212005. DOI
  36. Hu, S.; Wang, T.; Lu, B.; et al. Ionic-liquid-assisted synthesis of FeSe-MnSe heterointerfaces with abundant Se vacancies embedded in N,B co-doped hollow carbon microspheres for accelerating the sulfur reduction reaction. *Adv. Mater.* **2022**, 34, e2204147. DOI
  37. Wu, X.; Xie, R.; Cai, D.; et al. Engineering defect-rich bimetallic telluride with dense heterointerfaces for high-performance lithium-sulfur batteries. *Adv. Funct. Mater.* **2024**, 34, 2315012. DOI
  38. Li, H.; Chen, S.; Jia, X.; et al. Amorphous nickel-cobalt complexes hybridized with 1T-phase molybdenum disulfide via hydrazine-induced phase transformation for water splitting. *Nat. Commun.* **2017**, 8, 15377. DOI PubMed PMC
  39. Qi, K.; Cui, X.; Gu, L.; et al. Single-atom cobalt array bound to distorted 1T MoS<sub>2</sub> with ensemble effect for hydrogen evolution catalysis. *Nat. Commun.* **2019**, 10, 5231. DOI PubMed PMC
  40. Yu, Y.; Nam, G. H.; He, Q.; et al. High phase-purity 1T'-MoS<sub>2</sub>- and 1T'-MoSe<sub>2</sub>-layered crystals. *Nat. Chem.* **2018**, 10, 638-43. DOI
  41. Shi, Z.; Ding, Y.; Zhang, Q.; Sun, J. Electrocatalyst modulation toward bidirectional sulfur redox in Li-S batteries: from strategic probing to mechanistic understanding. *Adv. Energy. Mater.* **2022**, 12, 2201056. DOI
  42. Ye, Z.; Jiang, Y.; Li, L.; Wu, F.; Chen, R. Synergetic anion vacancies and dense heterointerfaces into bimetal chalcogenide nanosheet arrays for boosting electrocatalysis sulfur conversion. *Adv. Mater.* **2022**, 34, e2109552. DOI
  43. Li, G. R.; Gao, X. P. Low-cost counter-electrode materials for dye-sensitized and perovskite solar cells. *Adv. Mater.* **2020**, 32, e1806478. DOI PubMed
  44. Deng, T.; Wang, J.; Zhao, H.; et al. Dynamically regulating polysulfide degradation via organic sulfur electrolyte additives in lithium-sulfur batteries. *Adv. Energy. Mater.* **2024**, 14, 2402319. DOI
  45. Li, Z.; Li, P.; Meng, X.; Lin, Z.; Wang, R. The interfacial electronic engineering in binary sulfiphilic cobalt boride heterostructure nanosheets for upgrading energy density and longevity of lithium-sulfur batteries. *Adv. Mater.* **2021**, 33, e2102338. DOI
  46. Wang, J.; Yi, S.; Liu, J.; et al. Suppressing the shuttle effect and dendrite growth in lithium-sulfur batteries. *ACS. Nano.* **2020**, 14, 9819-31. DOI
  47. Zhang, L.; Liu, D.; Muhammad, Z.; et al. Single nickel atoms on nitrogen-doped graphene enabling enhanced kinetics of lithium-sulfur batteries. *Adv. Mater.* **2019**, 31, e1903955. DOI
  48. Li, H.; Xi, K.; Wang, W.; Liu, S.; Li, G.; Gao, X. Quantitatively regulating defects of 2D tungsten selenide to enhance catalytic ability for polysulfide conversion in a lithium sulfur battery. *Energy. Storage. Mater.* **2022**, 45, 1229-37. DOI
  49. Noorden R. The rechargeable revolution: a better battery. *Nature* **2014**, 507, 26-8. DOI PubMed
  50. Wang, M.; Fan, L.; Sun, X.; et al. Nitrogen-doped CoSe<sub>2</sub> as a bifunctional catalyst for high areal capacity and lean electrolyte of Li-S battery. *ACS. Energy. Lett.* **2020**, 5, 3041-50. DOI
  51. Liu, Y. T.; Liu, S.; Li, G. R.; Yan, T. Y.; Gao, X. P. High volumetric energy density sulfur cathode with heavy and catalytic metal oxide host for lithium-sulfur battery. *Adv. Sci.* **2020**, 7, 1903693. DOI PubMed PMC
  52. Zhang, G.; Feng, L.; Yu, J.; Wang, S. Full potential catalysis of Co<sub>0.4</sub>Ni<sub>1.6</sub>P-V/CNT with phosphorus vacancies for Li<sub>2</sub>S<sub>1.2</sub> deposition/decomposition and S<sub>8</sub>/Li<sub>2</sub>S<sub>n</sub> (3 ≤ n ≤ 8) conversion in Li-S batteries. *ACS. Appl. Mater. Interfaces.* **2023**, 15, 49170-80. DOI
  53. Hu, S.; Huang, X.; Zhang, L.; et al. Vacancy-defect topological insulators Bi<sub>2</sub>Te<sub>3-x</sub> embedded in N and B Co-doped 1D carbon nanorods using ionic liquid dopants for kinetics-enhanced Li-S batteries. *Adv. Funct. Mater.* **2023**, 33, 2214161. DOI
  54. Cheng, H.; Shen, Z.; Liu, W.; et al. Vanadium intercalation into niobium disulfide to enhance the catalytic activity for lithium-sulfur batteries. *ACS. Nano.* **2023**, 17, 14695-705. DOI